Building Simulation 2005

Ninth International IBPSA Conference
Montréal, Canada
August 15-18, 2005

SKY LUMINANCE MAPPING FOR COMPUTATIONAL DAYLIGHT MODELING

Bojana Spasojević and Ardeshir Mahdavi
Department of Building Physics and Building Ecology
Vienna University of Technology
Austria

ABSTRACT

Building design and control applications can benefit from daylight simulation. Currently, most daylight simulation applications work with simplified sky luminance models. However, reliable prediction of daylight availability in indoor environments via computational simulation requires reasonably detailed and accurate sky luminance models.

As past research has demonstrated, relatively low-cost sky luminance mapping via digital imaging can provide an alternative to high-end research-level sky scanners and thus support the provision of information on sky luminance distribution patterns on a more pervasive basis.

This paper explores the potential of using a digital camera with a fish-eye converter toward real-time derivation of sky luminance distribution maps. To explore the feasibility of this approach, sky luminance data derived from digital images were compared to the corresponding photometric measurements. To further calibrate the process, a correction factor was applied to the digitally gained luminance values. This correction factor was derived as the ratio of the optically measured to the digitally derived horizontal illuminance levels due to the sky dome.

The results show that digital sky imaging calibrated with parallel measurements of overall horizontal illuminance levels can provide a reliable basis for the generation of sky models for daylight prediction tools. Thus, the reliability of daylight simulation may be increased and simulation-based daylight-responsive lighting systems control methods in buildings can be enhanced.

INTRODUCTION

The availability and quality of daylight in indoor environments is amongst the primary concerns of good architectural design. Daylight simulation applications can help designers test and improve alternative daylight solutions. Moreover, daylight simulation can assist model-based building systems control applications (Mahdavi 2001, Mahdavi et al. 1999).

Currently, most daylight simulation applications work with simplified (e.g. uniform, isotropic) sky luminance models. The standard sky models created by using these tools do not represent the actual state of daylight availability accurately (Igawa et al. 1999). Such models are not sensitive to luminance variations in different areas of the sky. But the illuminance level at a point in a room is directly affected by the luminance of the sky area visible from that point, while the other parts of the sky contribute to the indoor illuminance only via reflection (Tregenza and Waters 1983).

Reliable prediction of daylight availability in indoor environments via computational simulation requires reasonably detailed and accurate sky luminance models. Moreover, such models, to be effective for design support purposes must be established for various locations over a statistically representative period of time. Toward this end, sky luminance mapping provides the empirical basis. As past research has demonstrated (Roy et al. 1998), relatively low-cost sky luminance mapping via digital imaging can provide an alternative to high-end research-level sky scanners and thus support the provision of information on sky luminance distribution patterns on a more pervasive basis.

This paper explores the potential of using a digital camera with a fish-eye converter toward real-time derivation of sky luminance distribution maps. Toward this end, sky luminance data derived from digital images were compared to the corresponding photometric measurements.

APPROACH

A fisheye lens makes it possible to capture sky images covering a 180° angle. A *Java* metadata extractor facilitates the extraction of RGB values out of a JPG image as well as camera values like shutter speed, f-stop number and ISO number. These extracted metadata are then used to derive luminance levels of a particular sky patch (Roy et al. 1998).

To examine the reliability of camera-driven sky luminance maps, a digital camera, equipped with a fisheye converter and pointing toward sky zenith, was placed on the roof of a building of the Vienna University of Technology, Vienna, Austria. In the images that have been taken from this point, 95% of the sky dome is unobstructed. Next to the camera, a sky monitoring device was located. The sky monitoring device consists of a box subdivided into 12 black-colored cells arranged in three levels. Each cell hosts an illuminance sensor measuring the horizontal illuminance reaching the sensor through a quadratic aperture. Due to the arrangement of the cells within the box and positioning of the 12 apertures, each sensor is exposed to the light coming from one of the 12 equally-sized (solid angle=π/6) sky hemisphere sectors (Figure 1).

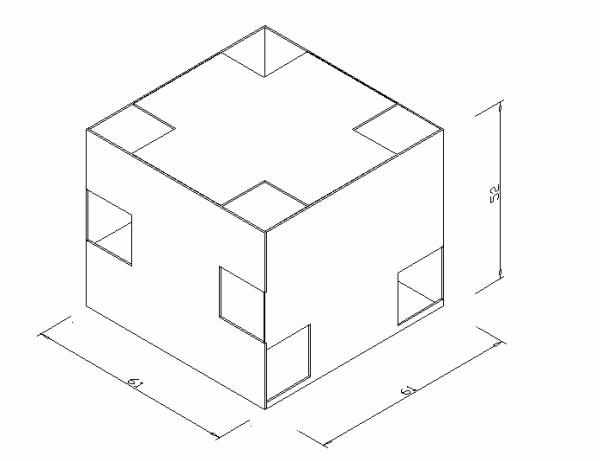

Figure 1 Monitoring device for measuring the illuminance due to 12 sky hemisphere sectors

A total of 170 images were collected using the camera during a week in July 2003. These were taken under sky conditions ranging from partly cloudy with brighter circumsolar region to turbid overcast. Simultaneously, the illuminance due to the 12 equally-sized sky sectors was measured using the aforementioned sky monitoring device. Additionally, the illuminance due to the entire sky dome was measured using a separate precision illuminance meter.

The distortion, occurring in the fisheye images, is caused by the equidistant transformation within the fisheye lens: the ratio of the angular distance of a point on the sky dome from the zenith to the altitude of the zenith (90°) corresponds to the ratio of the radial distance of the point's horizontal projection from the center of the fisheye image to the image radius:

$$\frac{Z}{90°} = \frac{l}{r} \qquad (1)$$

Where:

Z	angular distance of a point on the sky dome from the zenith
l	radial distance of the point's horizontal projection from the center of the fisheye image
r	image radius

Using this basic principle, the twelve sectors of the sky hemisphere, which affect the respective illuminance sensors within the sky monitoring device, were mapped onto the corresponding sectors in the JPG images (see figures 2 to 4).

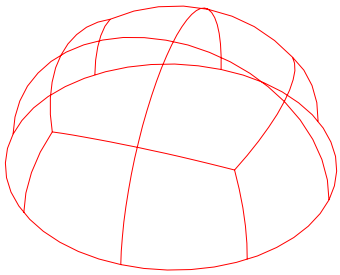

Figure 2 Twelve sectors of the sky dome

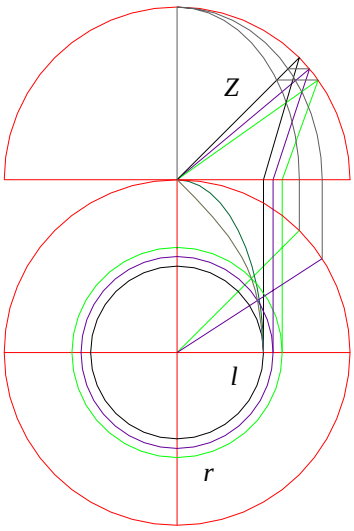

Figure 3 Equidistant transformation

Figure 4 Projection of 12 sectors on a fisheye image

The following algorithm (see equations 2 to 4, Roy et al. 1998) was used to derive the luminance of the particular sky portions from the extracted RGB values for each pixel and camera metadata values,

$$E_v = 0.895 \cdot \pi \cdot S \cdot T \cdot f^{-2} \quad (2)$$

$$V = 0.2125 \cdot R + 0.7154 \cdot G + 0.0721 \cdot B \quad (3)$$

$$L = 344.6 \cdot 10^{-6} \cdot V^{2.4} \cdot E_v^{-1} \quad (4)$$

Where:

R, G, B	RGB values for each pixel [0-255]
E_v	exposure value *L*
V	luminance related function
L	luminance of the sky patch [cd·m^{-2}]
S	ISO number
T	shutter speed [s]
f	f-stop number

Contribution of the luminance of a certain part of the sky hemisphere to the horizontal illuminance on a point in the center of the hemisphere (cp. Figure 5) depends on the altitude of a sky patch and differential solid angle subtended by that sky patch (Ashdown 1998):

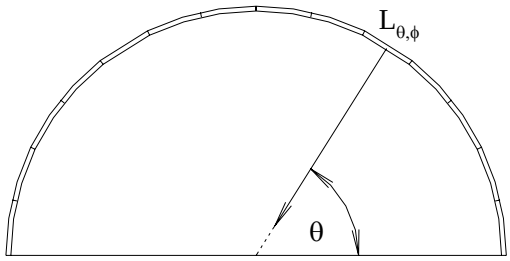

Figure 5 Sky patch luminance contribution to the global horizontal illuminance

$$E_i = L_i \cdot \sin\theta_i \cdot \Delta\Omega_i \quad (5)$$

The differential solid angle can be expressed in terms of angular size of the sky patch in altitudinal and azimuth direction (Szirmay-Kalos 1999):

$$\Delta\Omega_i = \cos\theta_i \cdot \Delta\varphi_i \cdot \Delta\theta_i \quad (6)$$

Where:

E_i	illuminance on a horizontal plane due to a particular sky patch
L_i	luminance of a sky patch
θ_i	altitude of the sky patch center
$\Delta\Omega_i$	differential solid angle of a sky patch
$\Delta\varphi_i$	angular size of a patch in azimuth direction
$\Delta\theta_i$	angular size of a patch in altitudinal direction

Combining the above equations, we obtain:

$$E_i = L_i \cdot \sin\theta_i \cdot \cos\theta_i \cdot \Delta\theta_i \cdot \Delta\varphi_i \quad (7)$$

Respectively, the total horizontal illuminance on a point in the center of the hemisphere consisting of the patches with known luminances can be calculated as follows (Tregenza and Waters 1983):

$$E = \int_0^{2\pi} \int_0^{\pi/2} L_{\theta,\varphi} \cdot \sin\theta \cdot \cos\theta \, d\varphi \, d\theta \quad (8)$$

Where:

E	global illuminance on a horizontal plane
$L_{\theta,\varphi}$	luminance of a sky patch with altitude θ and azimuth φ

As such, smaller patch sizes can increase the precision of the integration. In the present contribution, the sky dome was subdivided into 256 patches as per Figure 6.

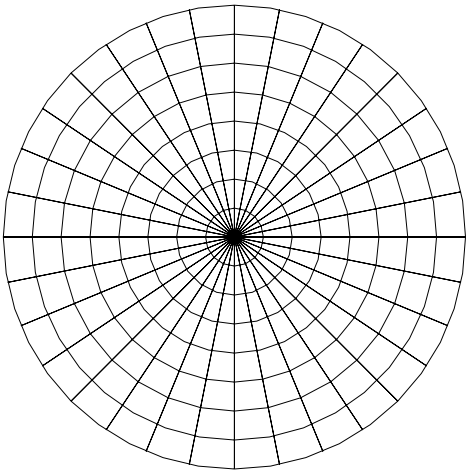

Figure 6 Segmentation pattern used for derivation of patch luminance values from digital sky images

To compare camera-based and photometric data, the camera-based illuminance values due to these 256 patches were aggregated in terms of the 12 aforementioned sky sectors (see Figure 2 and 4).

RESULTS

Figure 7 shows the relationship between illuminances due to the 12 aforementioned sky sectors as:

a) extracted from 170 camera-images (horizontal axis)
b) obtained, simultaneously, via photometric measurements (vertical axis) using the sky monitoring device (Figure 2).

Various factors (e.g. patch size and orientation, number of sky patches considered, distortion of the fisheye images in the lower areas of the sky hemisphere, errors in calculating the illuminance due to the sky areas closer to the horizon) can affect the accuracy of the camera-based horizontal illuminance due to a particular sky sector. Still, the correlation coefficient (r^2) of the corresponding linear regression amounts to 0.92.

To further calibrate the process, a correction factor was applied to the digitally gained illuminance values. This correction factor was derived as the ratio of the optically measured horizontal illuminance level due to the entire sky dome (E_{total}) to the sum of the 12 camera-based horizontal illuminance levels due to the 12 previously mentioned sky dome sectors (E_1 to E_{12}):

$$CF = \frac{E_{total}}{(E_1 + E_2 + ... + E_{12})} \quad (9)$$

Figure 8 shows the relationship between illuminances due to the 12 sky patches as:

a) corrected camera-based values (horizontal axis) and
b) photometric measurements (vertical axis).

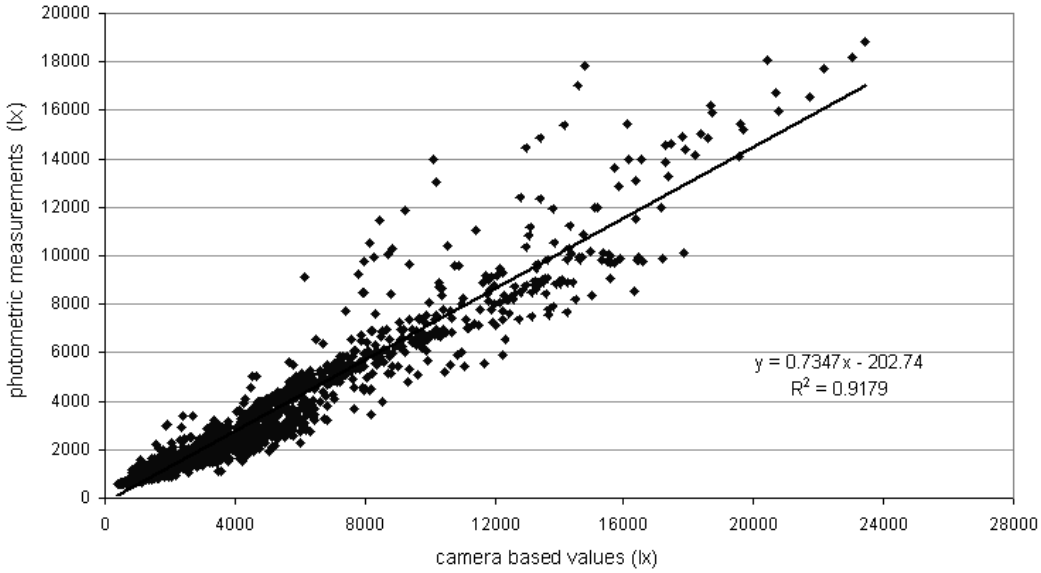

Figure 7 Photometrically measured versus camera-based illuminance values

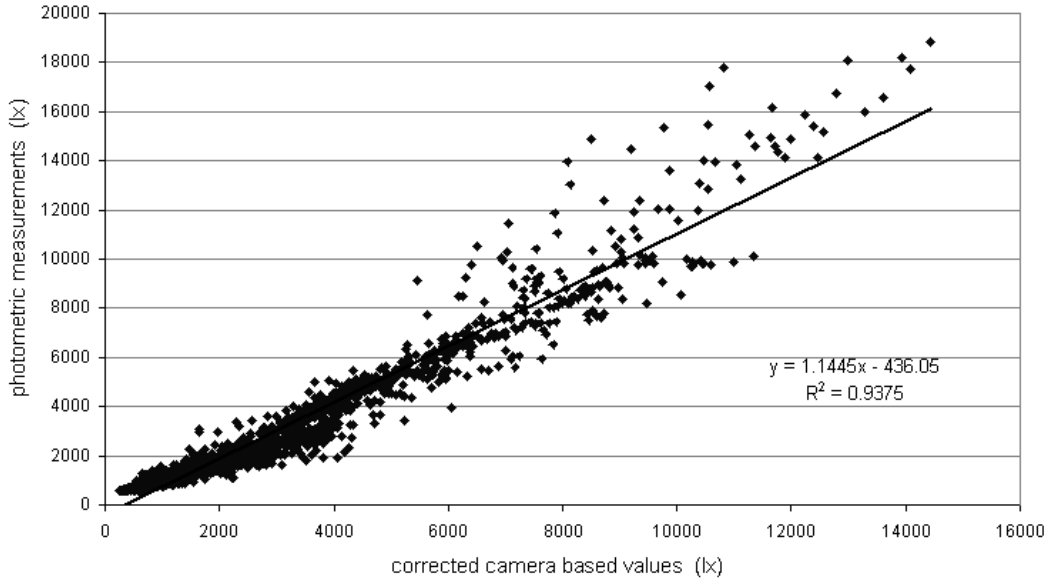

Figure 8 Photometrically measured versus corrected camera-based illuminance values

The correlation coefficient (r^2) of the corresponding linear regression amounts in this case to 0.94. Such a correction factor can be thus applied to the data gained through digital photography in order to provide more accurate patch luminance values for daylight simulation applications.

DISCUSSION

Digital imaging, combined with parallel photometric calibration, appears to provide a valuable means for a real-time generation of sky luminance maps. Such maps can be used as an input for a lighting simulation program to predict the indoor light levels for building design and control purposes. To illustrate the potential of this approach toward improved indoor light level simulation, we present the results of a comparison between two sets of lighting simulations to predict indoor illuminance levels in a test space under overcast sky conditions. As the test space, we selected an office in a university building (Vienna University of Technology) with two casement windows facing south-east (Figure 9).

The first set of simulations was conducted using the CIE standard overcast sky (Hopkinson et al. 1966, Moon and Spencer 1942) as the underlying sky model. In the second set, camera-based sky luminance data (from the prevailing – overcast – sky conditions at the time of indoor illuminance measurements) were used. In both cases, sky luminance data were normalized based on the measured global illuminance level due to the sky hemisphere. All other simulation model assumptions (e.g. room, surface reflectance, glazing transmittance, room furniture, measurement points) were identical.

Simulations were performed using lighting simulation program *LUMINA* (PalandMahdavi1999), for ten measurement points and five different times. Corresponding indoor illuminance measurements (for the same measurement points and time instances) were performed using a set of 10 illuminance sensors.

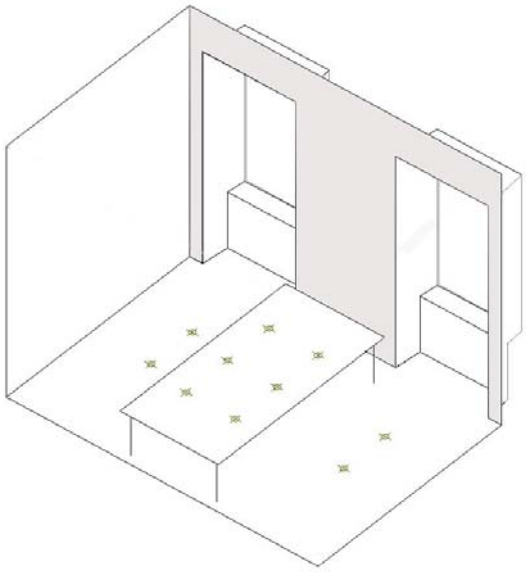

Figure 9 Illustration of the test space at the Vienna University of Technology with the measurement points

Figure 10 illustrates the linear regression between simulated illuminance values (horizontal axis) and measured indoor illuminance values (vertical axis) based on the CIE standard overcast sky. The correlation factor (r^2) amounts to 0.65.

The comparison between the simulation results with the application of the camera-based sky luminance mapping and simultaneously measured indoor illuminance values resulted in correlation factor (r^2) of 0.89 for the corresponding linear regression (Figure 11).

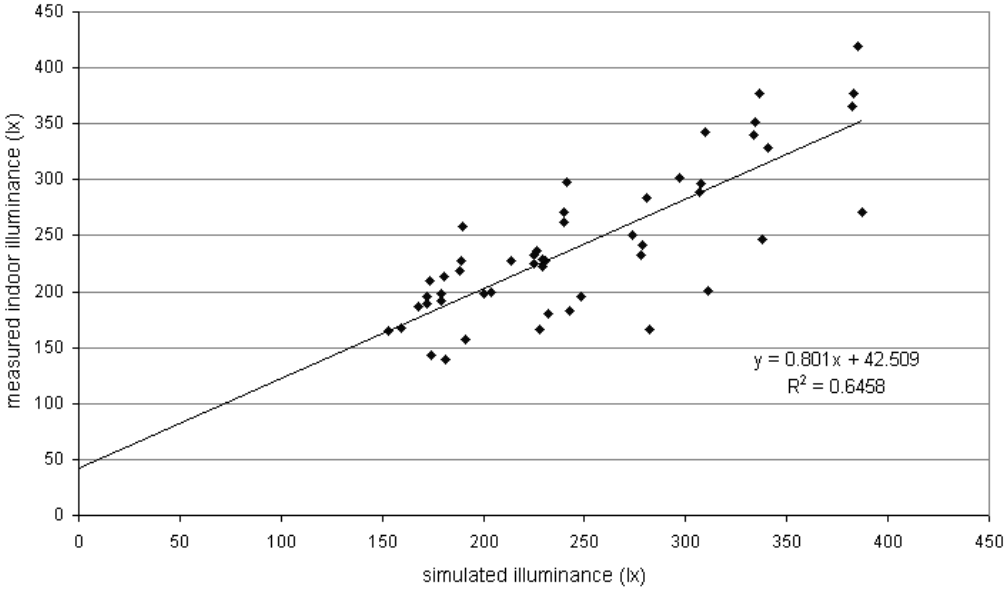

Figure 10 Measured versus simulated indoor illuminance values (sky luminance data based on CIE overcast sky model)

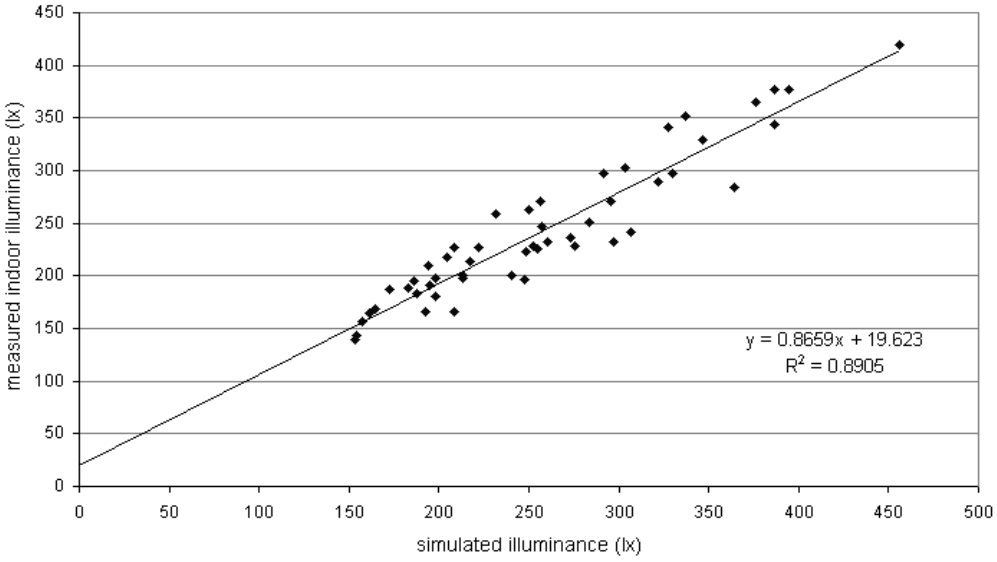

Figure 11 Measured versus simulated indoor illuminance values (sky luminance data based on digital imaging)

CONCLUSION

The results of the research presented in this paper imply that digital sky imaging calibrated with parallel measurements of overall horizontal illuminance levels, can provide an efficient basis for the generation of detailed sky luminance models. The application of such sky luminance models increases the predictive accuracy of the computational daylight prediction tools. Thus, the reliability of daylight simulation can be increased toward supporting the design and operation of daylighting systems in buildings.

ACKNOWLEDGMENT

The research described in this paper has been supported by *Bertha von Suttner* grant from *Austrian Exchange Service (ÖAD)* and a grant from *Austrian Science Fund (FWF),* project number P15998-N07.

REFERENCES

Ashdown, I. 1998. The Virtual Photometer: Modeling the Flow of Light. Publication copy, Ledalite Architectural Products Inc.

Hopkinson, R. G., Peterbridge, P., Longmore, J. 1966. Daylighting. Heinemann, London.

Igawa, N., Nakamura, H., Matsuura, K. 1999. Sky Luminance Distribution Model for Simulation of Daylit Environment. Proceedings of International Building Simulation (IBPSA) Conference '99, Volume 2: pp. 969 – 975.

Mahdavi, A. 2001. Simulation-based control of building systems operation. Building and Environment. Vol. 36, No. 6, ISBN: 0360-1323. pp. 789 – 796.

Mahdavi, A., Chang, S., Pal, V. 1999. Simulation-based integration of contextual forces into building systems control. Proceedings of Building Simulation '99. Sixth International IBPSA Conference. Kyoto, Japan. Vol. I. ISBN 4-931416-01-2. pp. 193 – 199.

Moon, P. and Spencer, D.E. 1942, Illumination from a non-uniform sky, Illum. Eng., Vol. 37, No. 10, pp. 707-726

Pal, V. and Mahdavi, A. 1999. A comprehensive approach to modeling and evaluating the visual environment in buildings. Proceedings of Building Simulation '99. Sixth International IBPSA Conference. Kyoto, Japan. Vol. II. ISBN 4-931416-02-0. pp. 579 – 586.

Roy, G.G., Hayman, S., Julian, W. 1998. Sky Modeling from Digital Imagery. ARC Project A89530177, Final Report. The University of Sydney, Murdoch University, Australia

Szirmay-Kalos, L. 1999. Monte-Carlo methods in global illumination. Institute of Computer Graphics, Vienna University of Technology.

Tregenza, P. and Waters, I. M. 1983. Daylight coefficients. Lighting Research and Technology. Vol. 15, No. 2, pp. 65 – 71.